Front. Struct. Civ. Eng. 2023, 17(4): 637–648
https://doi.org/10.1007/s11709-023-0902-0

RESEARCH ARTICLE

# Chloride diffusion in concrete with carbonated recycled coarse aggregates under biaxial compression

**Jingwei YING[a,b*], Weibeng WANG[b,c], Jianzhuang XIAO[d]**

[a] *Key Laboratory of Disaster Prevention and Structural Safety of Ministry of Education, Guangxi University, Nanning 530004, China*
[b] *College of Civil Engineering and Architecture, Guangxi University, Nanning 530004, China*
[c] *Guangxi Key Laboratory of Disaster Prevention and Engineering Safety, Guangxi University, Nanning 530004, China*
[d] *Department of Structural Engineering, College of Civil Engineering, Tongji University, Shanghai 200092, China*
[*] *Corresponding author. E-mail: yingjingwei@gxu.edu.cn*



**ABSTRACT** Chloride attack on concrete structures is affected by the complex stress state inside concrete, and the effect of recycled aggregates renders this process more complex. Enhancing the chloride resistance of recycled concrete in a complex environment via carbonization facilitates the popularization and application of recycled concrete and alleviates the greenhouse effect. In this study, the chloride ion diffusion and deformation properties of recycled concrete after carbonization are investigated using a chloride salt load-coupling device. The results obtained demonstrate that the chloride ion diffusivity of recycled concrete first decreases and then increases as the compressive load increases, which is consistent with the behavior of concrete, in that it first undergoes compressive deformation, followed by crack propagation. Carbonation enhances the performance of the recycled aggregates and reduces their porosity, thereby reducing the chloride diffusion coefficient of the recycled concrete under different compressive load combinations. The variation in the chloride ion diffusivity of the carbonized recycled aggregate concrete with the load is consistent with a theoretical formula.

**KEYWORDS** recycled concrete, carbonated recycled coarse aggregate, biaxial compression, chloride diffusion, stress level

## 1 Introduction

Owing to China's economic development, the transformation scale of old urban buildings is gradually increasing, and at least 1.8 billion tons of construction waste is generated annually [1]. The conventional method to manage such wastes is to use a simple landfill. Landfills require time-consuming processes, may occupy large areas of land, and cause secondary pollution. Using crushed construction waste as a recycled aggregate can reduce environmental pollution and allow the secondary utilization of construction waste [2]. However, because of defects in the original recycled aggregates, cracks develop earlier in recycled concrete than in natural concrete [3]. In addition, the old mortar attached to the surface of the recycled aggregate affects the interface transition zone (ITZ) and micropore structure distribution in the recycled concrete, thus significantly deteriorating the mechanical properties of recycled concrete [4,5]. In fact, defects in the ITZ significantly contribute to the unsatisfactory mechanical properties and durability of recycled concrete [6]. For example, weak ITZ structures and numerous microcracks are present in the old mortar of recycled aggregates, which reduce the strength of recycled concrete [7–10]. Therefore, appropriate measures must be undertaken to ensure sufficient strength and durability in recycled concrete.

As an important component of concrete, recycled aggregates significant affect the chloride diffusivity of concrete. A few studies [11–14] demonstrated that as the

*Article history: Received Jul 5, 2022; Accepted Sep 4, 2022*

replacement rate of recycled aggregates increased, the chloride ion penetration resistance of recycled concrete decreased. Meanwhile, other studies demonstrated that the chloride ion diffusion coefficient of recycled concrete increased with the degree of damage under freeze–thaw cycles and high temperatures [15,16]. Various methods have been investigated to improve the performance of recycled concrete, including adding fly ash and soaking recycled aggregates in water glass, lime solution, or a slurry composed of nano-$SiO_2$ [17–22]. Furthermore, carbonation enhancement is considered an effective method for enhancing the properties of recycled concrete. Singh et al. [23] compared water curing and carbonation curing and discovered that the compressive strength of carbonated concrete was higher than that of concrete cured in water. This provides a new concept for the curing of recycled concrete, as $CO_2$ can react with cement and cement hydration products to form $CaCO_3$ and amorphous silica gel, thereby reducing the porosity and water absorption of recycled aggregates [24–27]. Recycled concrete synthesized using carbonized recycled aggregates demonstrates higher chloride diffusion resistance than the typical recycled concrete [28–31]. In the durability test of recycled concrete, the effect of mechanical load is not considered. However, in practical engineering, the transmission of chloride ions into concrete is complex. For example, cracks caused by mechanical loading can accelerate the transmission of chloride ions in concrete. Previous studies showed that the effect of cracks on chloride diffusion in concrete depends primarily on the width and density of the cracks. As the crack width and density increase, the diffusion coefficient of chloride ions increases as well [32–34]. However, the diffusion of chloride ions along the crack direction decreases as the crack opening widens [35]. Although the shape of the crack imposes some effects during early chloride diffusion, it does not significantly affect chloride diffusion in the long term [36]. These studies regarding the effect of cracks on chloride ion diffusion primarily involved prefabricated cracks and did not account for the effect of mechanical loads.

A forced load can easily result in deformation and cracking in the concrete, which consequently affect chloride ion diffusion. In general, the chloride diffusion coefficient of concrete decreases and then increases as pressure increases. Moreover, the critical stress level of natural concrete (where the chloride ion resistance of concrete reaches the optimal stress level) is generally 0.3 [37–40], and the critical stress level of recycled concrete is 0.5–0.6 [41]. Although chloride diffusion in concrete under uniaxial compression has been investigated extensively, studies regarding chloride diffusion in concrete under biaxial compression are few and involved restrictions. For example, the study of Hong et al. [42] was performed under a preload load instead of a continuous compression load. Cheng et al. [43] adopted the natural diffusion method, which required a long test duration and can only accommodate a maximum stress level of 0.3. Hence, the results obtained did not include the chloride diffusion coefficient of concrete under high stress levels. In practical engineering, the non-uniformity of a material results in complex stress states inside concrete, i.e., tension and compression stress states of concrete under uniaxial and biaxial stresses. Primary defects in recycled concrete lead to a more complex erosion environment than those in natural aggregate concrete. In this study, a custom-developed chlorine–salt load-coupling device is used. A chloride ion diffusion test is performed under a continuous compressive load, and the test cycle is reduced by electrically accelerating ion migration.

In this study, three types of recycled aggregates are obtained via mechanical crushing and strengthening using carbon dioxide. Subsequently, various recycled aggregates are poured into recycled concrete, and their chloride diffusion properties under uniaxial and biaxial compressive loads are tested using a chloride load-combination device. The micropore structure of the concrete is tested using mercury intrusion porosimetry and further analyzed in terms of its effect on chloride ion diffusion in concrete. Finally, the strain distribution on the surface of the concrete is obtained using the digital image correlation method (DIC), and the effect of loads on the chloride diffusion of recycled concrete is investigated based on the strain distribution at the microscale.

## 2 Experimental program

### 2.1 Materials and sample preparation

The cement used in this study was ordinary Portland cement with a compressive strength of 42.5 MPa. Natural river sand was used as fine aggregates. Three types of recycled coarse aggregates (RCAs), named RCA1, RCA2, and RCA3, were synthesized from virgin concrete, and they exhibited water-to-cement ratios of 0.4, 0.5, and 0.6 after 28 d of standard curing. These natural aggregate concretes were tested in a laboratory, and the volume content of the natural aggregates was the same as that of the recycled aggregates. The RCAs were synthesized by manually crushing virgin concrete using a hammer, followed by crushing using a jaw crusher. Finally, three types of recycled aggregates with particles sizes of 5–20 mm were obtained after screening and cleaning.

The three types of RCAs, i.e., RCA1, RCA2, and RCA3, were carbonized under high pressure using a carbonization device. A schematic of the carbonization device is shown in Fig. 1. The carbonation process was as follows: First, the recycled aggregate was placed in a

carbonization cylinder under vacuum for 10 min. Subsequently, 99.9% $CO_2$ was injected into the carburizing equipment to stabilize the in-cylinder pressure to 0.5 MPa. Next, the carbonated recycled aggregates were removed every 24 h to monitor the progress of the carbonization. Three types of carbonated recycled coarse aggregates (CRCAs), denoted as CRCA1, CRCA2, and CRCA3, were obtained. Gradation curves for the CRCA obtained based on the Chinese testing method specified in JGJ 52-2006 [44] are shown in Fig. 2.

RCAs with carbonation times of 1, 3, and 7 d were randomly selected for splitting, and their surfaces were sprayed with phenolphthalein solution. Their carbonization progress was analyzed based on their color development. An old mortar that does not exhibit color changes indicates that the RCA has undergone carbonization. The color of the old mortar in the RCA after carbonization for 1, 3, and 7 d is shown in Fig. 3. Results based on color change in the phenolphthalein solution demonstrate that the carbonation depth of the aggregate increased as carbonization progressed. In this study, the authors primarily investigated the different properties of carbonized recycled aggregates and the concrete formed using them. Additionally, some of the test results obtained were compared with those of uncarbonized recycled aggregates and the concrete formed using them, as presented in Ref. [45].

The basic properties of the CRCAs and their comparison with those of uncarbonized RCAs are summarized in Table 1. For example, 1326 (↑1.1%) indicates that the bulk density of the CRCA is 1326 kg/m$^3$, which is 1.1% higher than that of the corresponding uncarbonized RCA. Based on the results summarized in the table, carbonization can increase the apparent density of the RCAs and reduce their water absorption and crushing index.

The mixture and 28-d cube compressive strength of the CRCAs are listed in Table 2. The water-to-binder ratio of all the specimens was 0.5, and the same cement and fine aggregates were used. The CRCAs comprised various RCAs. For example, CRCA1 comprised RCA1. In the experiment, three different shapes and sizes of specimens were fabricated: cube, 100 mm × 100 mm × 100 mm; cuboid, 100 mm × 100 mm × 50 mm; and cylinder, Φ 100 mm × 50 mm.

## 2.2 Chloride diffusion

Two devices are primarily used to test the chloride diffusion coefficient of concrete. The first is the commonly used rapid chloride migration (RCM) device, whose test method is based on the Chinese standard (GB/T 50082-2009) [46]. The second is the chloride load-combination device invented by the author. A schematic

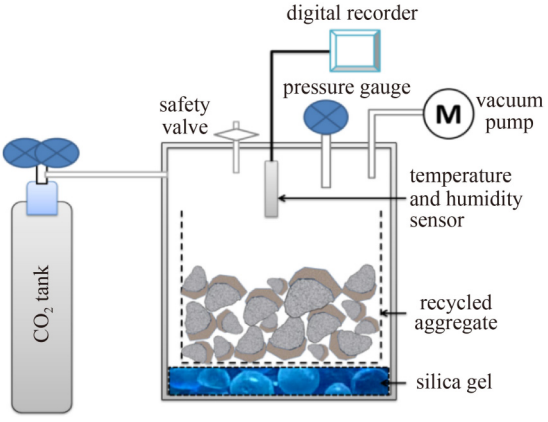


**Fig. 1** Schematic of carbonization device.

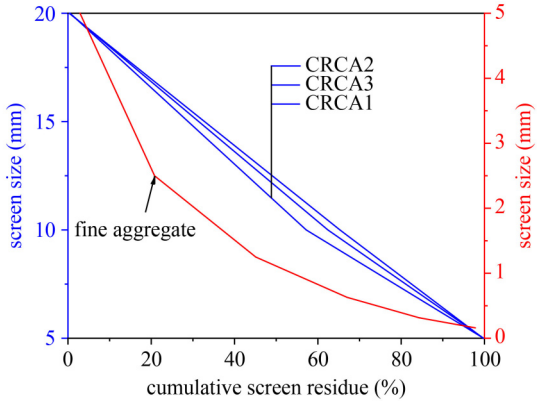


**Fig. 2** Grading curves of coarse and fine aggregates.

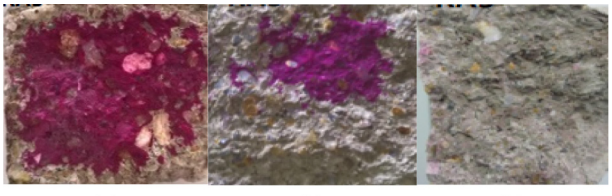


**Fig. 3** Carbonation depth of the regenerated aggregates under different carbonation durations: (a) after 1 d carbonization; (b) after 3 d carbonization; (c) after 7 d carbonization.

**Table 1** Properties of CRCAs and their changes relative to RCAs

| aggregate type | bulk density (kg/m$^3$) | apparent density (kg/m$^3$) | water absorption (%) | crushing index (%) | mud content (%) | needle-like content (%) | old mortar content (%) |
|---|---|---|---|---|---|---|---|
| CRCA1 | 1326 (↑1.1%) | 2696 (↑0.8%) | 3.17 (↓34.0%) | 15.26 (↓6.6%) | 1.71 (↓1.2%) | 7.9 (↓2.5%) | 45.96 |
| CRCA2 | 1309 (↑0.8%) | 2686 (↑0.6%) | 3.69 (↓29.0%) | 16.34 (↓7.3%) | 1.69 (↑0.6%) | 7.6 (↑1.3%) | 43.21 |
| CRCA3 | 1298 (↑0.9%) | 2681 (↑0.7%) | 4.14 (↓29.8%) | 17.21 (↓7.6%) | 1.72 (↑0.6%) | 7.8 (↑2.6%) | 41.63 |

of the chloride load-combination device is shown in Fig. 4.

The stress directions of the specimens are shown in the red coordinate axis in Fig. 4. The process involved in configuring the chloride load-combination device is as follows:

First, the concrete specimens after subjected to grinding and water saturation treatment were installed on the reaction frame. Next, a test piece was pressurized using an oil pump jack system. The loading speed was controlled to 0.5–1 MPa/s, and the lock valve fixed the oil pressure after pressurization. Sodium hydroxide solution was injected into the anode solution box, whereas NaCl solution was injected into the groundwater storage tank. A cathodic solution circulation circuit was connected to a rubber hose, and a constant-flow pump was connected to the cathodic solution box. The current and solution temperatures at different moments, such as the initial and termination, were recorded. At the end of the powering process, the specimens were cut in half and sprayed with silver nitrate. The chloride ion diffusion depth was measured after the color development. The chloride ion diffusion coefficient was calculated based on concrete durability specifications (GB/T 50082-2009) [46].

## 2.3 Stress level

In general, when the compressive stress of concrete reaches 75% of its ultimate strength, unstable cracks may appear [47]. In this study, three paths were loaded, where the compression load ratios in the *X*- and *Y*-direction were 1:0, 1:1, and 1:2. The stress level was defined as the ratio of the actual load to the ultimate load under the same loading path. For concrete specimens subjected to chloride ion diffusion under each pressure, five stress levels were designated: 0, 0.3, 0.5, 0.7, and 0.8.

**Table 2** Mix proportion of CRCA concrete

| specimen | material consumption (kg/m$^3$) | | | | | 28-d strength (MPa) |
|---|---|---|---|---|---|---|
| | *W/C* | cement | water | fine aggregate | CRCA | |
| CRCA1 | 0.5 | 404.7 | 202.3 | 701.2 | 1015.6 | 37.7 |
| CRCA2 | 0.5 | 406.1 | 203.1 | 703.7 | 1009.7 | 35.4 |
| CRCA3 | 0.5 | 407.4 | 203.7 | 705.8 | 1004.7 | 33.4 |

Note: To ensure the same volume content of coarse aggregates, the water consumption was adjusted based on the water content and water absorption of different coarse aggregates, and the free water content was set as the same for different mix proportions.

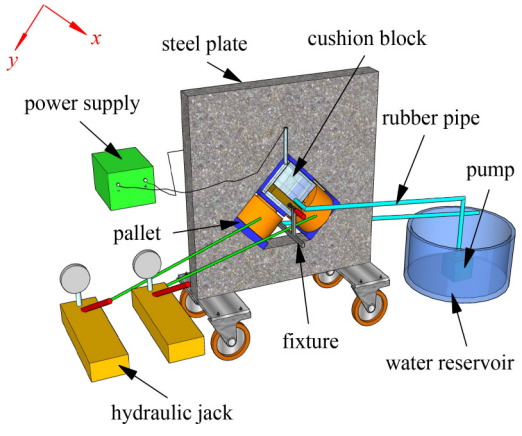


**Fig. 4** Schematic of chloride load-combination device invented by the authors.

## 2.4 Pore structure

To investigate the micropore structure of concrete, an automatic mercury porosimeter (AutoPore IV 9500, Micromeritics Instrument, USA) was used to measure the pore structure of concrete.

Based on the mix proportions listed in Table 2, the new mortar in the concrete and the old mortar were selected for the pore structure test. A specimen measuring approximately 5 mm was obtained using a cutting machine. The specimens were soaked in anhydrous ethanol for approximately 24 h and dried in a vacuum-drying tank. Finally, the pore structures of the specimens were tested based on the instruction for mercury intrusion porosimetry.

## 2.5 Digital image correlation method

Two-dimensional (2D) DIC technology can be used to analyze the displacement and strain fields on the surface of the concrete specimens. A speckle was created by spraying paint on the surface of the specimen to improve the measurement accuracy, as shown in Fig. 5.

Figure 6 shows a schematic of the test device used for this test. The test device comprised a load application system and a DIC non-contact strain system. The following processes were performed for the test.

The concrete specimens were mounted on a counterforce holder. To ensure the stability of the loading, an initial load of 2 MPa was applied to the

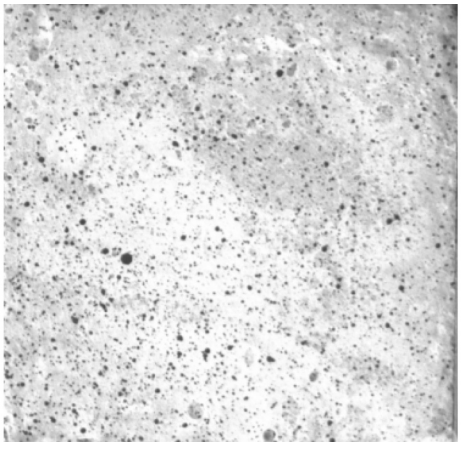

**Fig. 5** Speckle created using spray paint.

specimen. The position of the industrial camera used at high pixels was adjusted such that the optical axis was perpendicular to the surface of the specimen being tested. A compressive load was applied to the specimen via the set-loading method, and image acquisition was performed. Finally, the acquired images were analyzed using an image analysis software to obtain the strain field of the regenerated concrete generated at different stress levels during the entire loading process.

## 3 Test results and discussion

### 3.1 Pore structure

To analyze the effect of carbonization on the microporous structure of the old mortar, the old mortar in the RCA (RCAm) was compared with the old mortar in the CRCA (CRCAm). Figure 7 shows the cumulative intrusion and log differential intrusion curves of the CRCAm vs. the pore diameter. Table 3 lists the pore structure parameters of the old mortar in concrete. In the table, 7.83 (↓23.7%) indicates that its total porosity is 7.8%, which is 23.7% lower than that of the same type of uncarbonized mortar. Based on the results summarized in Table 3, the total porosities of RCAm1, RCAm2, and RCAm3 decreased by 23.7%, 23.5%, and 16.7%, respectively, after $CO_2$ curing and strengthening. The products yielded by carbonization occupied the large pores in the recycled aggregates; therefore, carbonization reduced the chloride ion diffusion coefficient of the recycled aggregate concrete. After carbonization, the pore diameters of RCAm1, RCAm2, and RCAm3 decreased by 57.9%, 36.7%, and 34.5%, respectively, the connectivity of the pores in the RCAs further reduced, and the tortuosity of the permeability path further increased, thus improving the overall impermeability of the recycled concrete. The apparent density of each old mortar under a pressure of 3.59 kPa (0.52 psia) can be measured via mercury intrusion porosimetry, as summarized in Table 3. Based on the figure, the apparent densities of RCAm1, RCAm2, and RCAm3 increased by 1.5%, 3.3%, and 6.4%, respectively, after carbonization. Consequently, the overall apparent density of the RCAs increased, which is consistent with the performance of the recycled aggregates.

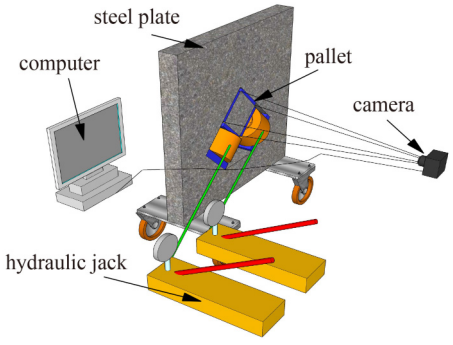


**Fig. 6** Schematic of DIC image acquisition device.

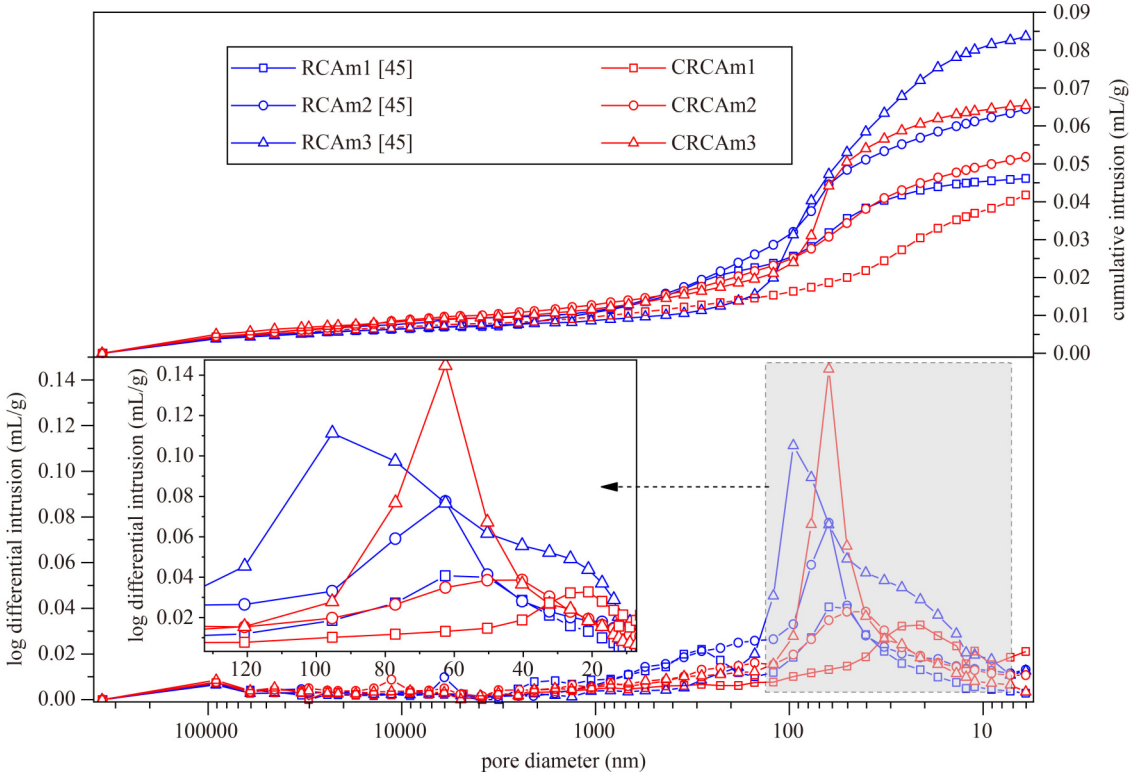


**Fig. 7** Pore size distribution of mortar for each sample.

In this study, the pore volume fraction with capillary porosity measuring between 30 and 10000 nm was defined [48], and the pore size of concrete was categorized into harmless pores (< 20 nm), less-harmful pores (20–50 nm), harmful pores (50–200 nm), and more-harmful pores (> 200 nm) [49]. Figure 8 shows the porosities of the mortars after and before carbonization. For example, ↓37% in the figure implies that the more-harmful porosity of the old mortar after carbonization is 37% lower than that before carbonization. The harmless and less-harmful pores did not significantly affect chloride diffusion, whereas the harmful and more-harmful pores exerted a more significant affect. Therefore, the variations in the harmful and more-harmful pores were analyzed. Based on the figure, the porosity of the harmful pores decreased after carbonization. In addition to CRCAm3, the more-harmful pores showed reduced porosity. In CRCAm3, the porosity of the more-harmful pores increased, whereas that of the harmful pores decreased. The porosity of the harmful pores constituted the largest proportion in CRCAm3, which resulted in a decrease in the total porosity of CRCAm3 after carbonization. This is consistent with the results obtained by Liang et al. [30]. After carbonization, the total porosities of the harmful and more-harmful pores in the recycled aggregate reduced, which improved the overall properties of the recycled concrete. This is because $CO_2$ can react with hydration products in the old mortar to generate larger carbonation products, e.g., $CaCO_3$ and silica gel [20,24,50], change the original pore size and pore shape in the old mortar, reduce old mortar's overall porosity, and improve the old and new ITZs [29].

**Table 3** Pore structure parameters of old mortar before and after carbonization

| specimen | total porosity (%) | most probable pore size (nm) | apparent density (g/mL) |
|---|---|---|---|
| CRCAm1 | 7.83 (↓23.7%) | 26.3 (↓57.9%) | 2.216 (↑1.5%) |
| CRCAm2 | 10.52 (↓23.5%) | 40.3 (↓36.7%) | 2.205 (↑3.3%) |
| CRCAm3 | 14.25 (↓16.7%) | 62.5 (↓34.5%) | 2.179 (↑6.4%) |

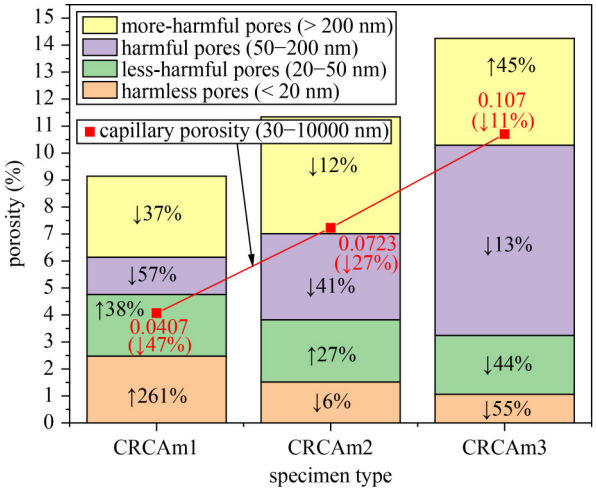


**Fig. 8** Pore size distribution and capillary porosity of mortar in each sample.

## 3.2 Digital image correlation analysis of concrete

Under different load combinations, the interior of the recycled concrete undergoes deformation and damage. To further analyze the effect of compressive load on the chloride diffusion of recycled concrete, the strain distribution diagram of recycled concrete under compression is presented in Fig. 9. The maximum tensile strain shown in the cloud diagram is 0.5%. The strain field shown in red in this region signifies that with a tensile strain exceeding 0.5%. Accordingly, the maximum compressive strain is set to −0.5%. The blank area is the area where exterior skin peeling or surface collapse

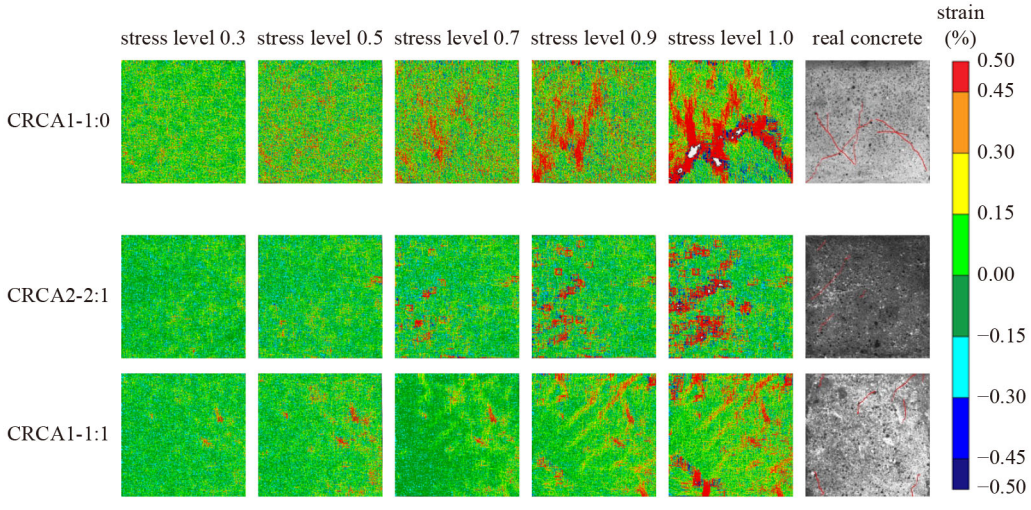


**Fig. 9** Strain field of each specimen under load.

occurred on the specimens. The strain cloud images corresponding to five stress states with stress levels of 0.3, 0.5, 0.7, 0.9, and 1.0 are selected for analysis. The last picture is the original picture showing a failed specimen. For example, CRCA1-1:1 indicates that the compression specimens are CRCA1, and the load ratio in the *X*- and *Y*-direction is 1:1. Owing to space limitations, the representative strain images are shown for each load ratio.

Based on the figure, in the compression concrete with a uniaxial stress level of 0.3, a few microcracks appeared because the bond strength between the cement mortar and CRCA was less than the tensile stress. Nevertheless, no severe damage or cracks occurred at this time, and most of the images appeared green or light green. When the stress level in the *Y*-direction was 0.5, more red dot distributions were indicated compared with when the level was 0.3, and the overall color showed a lighter shade of green (the tensile strain range was 0%–0.15%). When the stress level was 0.5, the specimens began to exhibit a local stress concentration and partial damage. However, in general, the pores of the concrete remained compressed, the effect of pore shrinkage on chloride diffusion was dominant, and the chloride diffusion coefficient remained relatively low. When the stress level in the *Y*-direction continued to increase to 0.7, the red dot distribution expanded. Microcracks developed gradually near the coarse aggregates, and most of the cracks were vertical cracks. The main strain field exhibited a strip and band distribution, which is similar to the crack development mode of recycled concrete reported by Li et al. [51] and Xiao et al. [52]. This indicates that the damage inside the concrete increased gradually, the cracks expanded, and new cracks were generated. The effect of crack generation on chloride ion diffusion was more significant than that of pore shrinkage, and the chloride ion diffusion coefficient increased. When the stress level reached 0.9, the size and number of cracks increased significantly and the red strip distribution was connected. The cracks inside the concrete exhibited significant cracks, which caused considerable damage. When the compression limit state was reached, a large area of cracks appeared in the specimens. Finally, the specimens were damaged owing to the large cracks along the loading direction, as shown in the last drawing.

The CRCA crack development model shows that the initiation and development of microcracks were affected by the relative strengths of the new and old ITZs, which is consistent with the findings of Li et al. [53]. Microcracks in the CRCA first appeared in the vicinity of the old and new ITZs. Subsequently, they developed further in the nearby old mortar area, and numerous cracks were generated owing to the difference in strength between the old and new ITZs. Cracks generally appear less in CRCA than in RCA. RCAs enhance the performance of concrete after carbonization and may generate $CaCO_3$ and silica gel products to occupy the pores. These factors improve the old and new ITZs and reduce the occurrence of cracks in concrete.

For biaxial compression, when the stress ratio in the *X*- to *Y*-directions was 2:1, the chloride diffusion coefficient of the CRCA decreased by 20%–30% compared with that of the RCA. Compared with that before carbonization, the chloride diffusion coefficient after carbonization decreased by 33.48%. Based on Fig. 9, when the stress level was 0.3, the image appeared primarily green. At this time, the pores and original microcracks in the concrete remained compressed, and when the stress level was 0.5, the strain field appeared green and light green; however, a local red dot distribution was indicated in the ITZ and the old mortar area. This shows that the pores and microcracks of the specimen in this state remained compressed, and that a stress concentration began to appear in the local weak area. When the stress level was 0.7, the stress concentration area further increased. The red dotted area was evenly distributed on the test piece, and the test piece was damaged. When the stress level was 0.8, the chloride diffusion coefficient of concrete increased and then decreased as compared with that for the case without load; however, in general, it was similar to that for the case without load. Under uniaxial compression, when the stress level was 0.7, the chloride diffusion coefficient of concrete was comparable to that of the case without load. This indicates that a bidirectional compressive load can improve the resistance of concrete to chloride ion penetration. Based on the analysis of the strain field distribution image when the stress levels were 0.9 and 1.0, the damage degree of the two specimens increased until crack or skin peeling occurred on the surface of the specimen. In addition, compared with the uniaxial compression, the tensile strain indicated primarily a stripping distribution, which was wider than the distribution under uniaxial compression. This shows that concrete was more fully utilized, and thus, the strength of concrete under biaxial compression was higher than that under uniaxial compression.

When the *X*- to *Y*-direction stress ratio was 1:1, the change in the chloride diffusion resistance of concrete was similar to that when the stress ratio was 2:1. Moreover, when the *Y*-direction stress level was lower than 0.5, the closer the applied *X*-direction load to the *Y*-direction load, the more evident was the effect of the concrete anti-chloride diffusion. However, when the stress ratio was 1:1 and the stress level was 0.7, the anti-chloride diffusion of the concrete was similar to that for the case without load. This might be because when the stress ratio was 1:1 and the stress level was low (less than 0.5), the resistance of concrete to chloride diffusion was more sensitive to the increase in the stress level. In this case, the internal pores of the concrete were compressed

earlier, and internal cracks developed earlier. Furthermore, based on Fig. 9, the red dot distribution appeared earlier when the *X*- to *Y*-direction stress ratio was 1:1 compared with when the stress ratio was 2:1.

In general, the decrease in the chloride diffusion coefficient under uniaxial compression was less than that under biaxial compression. This is because the pores and microcracks in the concrete reduced in the two directions under biaxial compression, thus causing the pore volume and microcrack area to further decrease. The diffusion of chloride ions in concrete was affected by the crack area and porosity [37,54]. Additionally, based on Fig. 9, under uniaxial compression, most of the cracks were strip cracks that had developed along the stress direction. Under biaxial compression, the cracks were short and evenly distributed.

### 3.3 Effect of biaxial compressive load on chloride diffusion in recycled concrete

Figure 10 shows the absolute value of the chloride ion diffusion coefficient for the case without load measured using the chloride load-combination and RCM test devices. For example, ↓24.8% indicates that the chloride diffusion coefficient of CRCA1 obtained using the chloride load-combination device is 18.85 × $10^{-12}$ $m^2/s$, which is 24.8% lower than that for the same type of concrete with uncarbonized RCAs. Furthermore, the figure shows that the chloride ion diffusion coefficient measured using the chloride load-combination device is similar to that measured using the RCM test device. Therefore, the results yielded by the chloride load-combination device can be considered reliable. In addition, the chloride ion diffusion coefficient of the CRCA after carbonation generally decreased by 20%–30% compared with that prior to carbonation. This might be due to the reduced porosity of the old mortar in the recycled aggregate and the improved performance of the ITZ. Thus, the initial porosity and microcracks in the recycled concrete composed of carbonized recycled aggregate reduced, and the chloride ion resistance enhanced. Notably, carbonation reduces the alkalinity of concrete, which affects the chloride ion binding capacity. In this study, the alkalinity of the new mortar was not reduced; only the alkalinity of the old mortar was reduced. Because the content of old mortar was extremely slight, the decrease in alkalinity in the old mortar barely affected the alkalinity of the concrete. The decrease in alkalinity in the old mortar adversely affected chloride ion binding, but the ITZ and old mortar of the recycled aggregate became denser after carbonization. Therefore, the effect of pore improvement on chloride ion transport was greater than that of reduced alkalinity. These findings are similar to those of Zhan et al. [55] and Chang [56].

All the relative values shown in Fig. 11 were calculated

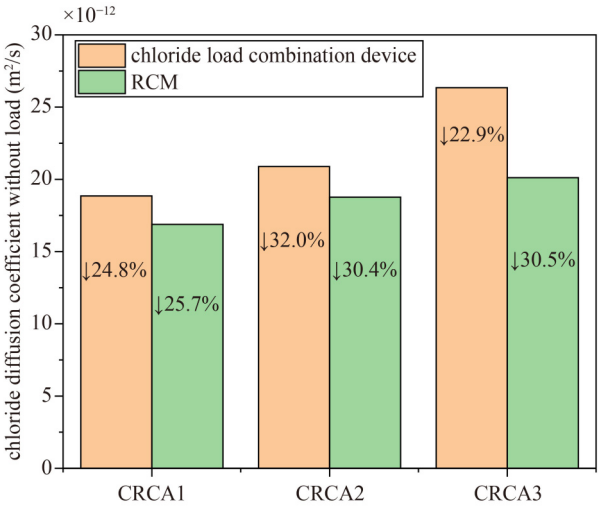


**Fig. 10** Absolute value of chloride diffusion coefficient for case without load.

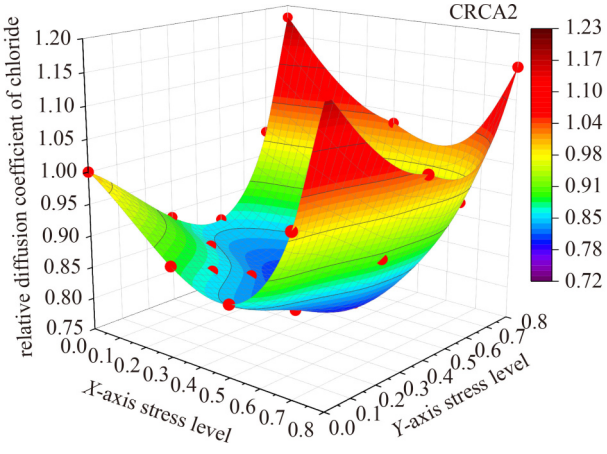


**Fig. 11** Three-dimensional graph of relative chloride diffusion coefficient (CRCA2).

based on the absolute values shown in Fig. 10. Figure 11 (CRCA2 specimens) shows the stress levels in two directions, one on the *X*-axis and the other on the *Y*-axis. The measured chloride ion diffusion coefficient (the ratio of the chloride ion diffusion coefficient for the case with load to that for the case without load) is depicted as a three-dimensional diagram on the *Z*-axis. The red dots indicate the values measured during the test.

Figure 12 shows a 2D cloud diagram of the relative chloride ion diffusion coefficient of each specimen under a biaxial compression load. Based on Fig. 12, when the stress level in the *X*- and *Y*-direction of the strengthened recycled concrete was lower than 0.5, the 2D cloud diagram of the relative value of the chloride ion diffusion coefficient was thinner than that before strengthening. This shows that the chloride diffusion coefficient of the strengthened CRCA changed more slowly with the stress

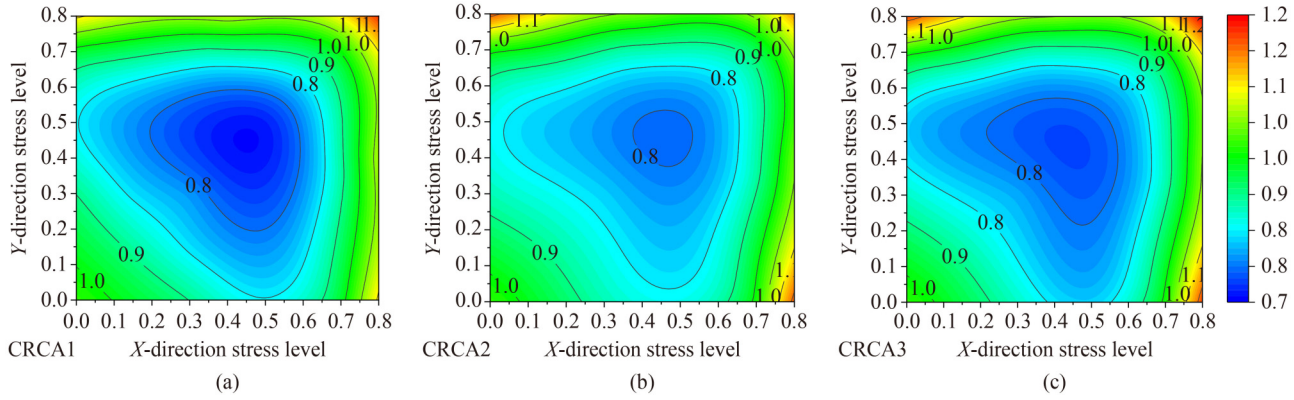


**Fig. 12** 2D cloud diagram of the relative value of chloride ion diffusion coefficient under biaxial compression load of each specimen: (a) CRCA1; (b) CRCA2; (c) CRCA3.

level. The sensitivity of chloride diffusion to compressive loads can be reduced to a certain extent via RCA strengthening. This is because of the presence of old mortar and a complex ITZ in the RCA before carbonization, and the abundance of initial pores and microcracks in the recycled concrete. Consequently, more pores and channels can be compressed under low stress, the chloride diffusion coefficient changes more rapidly, and the isoline distribution is denser. After carbonization, the porosity of the CRCA old mortar decreased, and the performance of the ITZ improved. The compressible initial porosity and microcracks in the CRCA reduced the sensitivity of the strengthened recycled concrete to compressive loads.

Furthermore, based on Fig. 12, under the effect of only the *X*- or *Y*-direction compressive load, the chloride ion diffusion coefficient of each concrete material first decreased with the stress level. The chloride diffusion coefficient of concrete under uniaxial compression was 17.01% lower than that of concrete without load. However, when the stress level reached approximately 0.5, the chloride ion diffusion coefficient increased with the stress level. This might be because when the stress level was low (less than 0.3), the original pores and microcracks perpendicular to the direction in which the load was exerted in the concrete reduced or vanished owing to the compressive load. The pores and microcracks parallel to the direction of load exertion remained unchanged, which reduced the overall porosity and pore connectivity in the concrete, thus hindering the penetration and diffusion of chloride ions. When the stress level is 0.3–0.5, a local stress concentration may occur in the concrete and microcracks; however, the resulting cracks will be small. At this time, the effect of pore compression on chloride ion diffusion is more significant than that of fracture; therefore, the chloride ion diffusion coefficient decreases, but the rate of decrease is lower. When the stress level was above 0.5, the microcracks began to accelerate the expansion and extension. Connected cracks can result in chloride diffusion channels and a rapid increase in the chloride diffusion coefficient.

For concrete with different mix proportions, a concave trend was indicated, as shown in Figs. 11 and 12. The stress levels in the *Y*- and *X*-direction at the concave point were approximately 0.5, and the chloride dissociation diffusion coefficient at this point was the lowest. The chloride diffusion coefficient of the concrete under biaxial compression was 26.05% lower than that of the concrete without load. For the same concrete mix proportion, the chloride diffusion coefficient in the concrete under biaxial compression was up to 11.04% lower than that under uniaxial compression. This shows that the chloride diffusion coefficient of concrete was further reduced by applying a compressive load in the *Y*- and *X*-direction simultaneously. However, when the stress levels in the *Y*- and *X*-direction increased equally, the chloride ion diffusion coefficient decreased. When the stress level continued to increase until a critical value, the chloride ion diffusion coefficient in the concrete increased with the stress level. When the stress levels in the *Y*- and *X*-direction reached approximately 0.7, the chloride diffusion coefficient was similar to that for the case without load. When the stress levels in the *Y*- and *X*-direction reached 0.8, the chloride diffusion coefficient under bidirectional compression exceeded that under the case without load. This might be because when the concrete material was simultaneously subjected to biaxial compression loads in the *Y*- and *X*-direction, the application of load in the *X*-direction compressed the internal cracks caused by the load in the *Y*-direction to a certain extent. Compressed cracks can prevent the expansion of concrete materials, delay concrete damage, and improve the chloride corrosion resistance of recycled concrete. However, when the stress on both sides increased significantly, microcracks caused by concrete damage dominated. At this time, the development of microcracks in the concrete was further accelerated, which reduced its resistance to chloride corrosion. In particular, when the stress levels in the *Y*- and *X*-direction

reached 0.8, the cracks between the ITZ inside the concrete and the matrix overlapped and connected [47]. The chloride ion diffusion coefficient at this time exceeded the chloride ion diffusion coefficient for the case without load.

The variation in the chlorile ion diffusion coefficient described above is consistent with the results of Hong et al. [42] and Cheng et al. [43]; however, they discovered that the stress level corresponding to the minimum chloride ion diffusion coefficient in concrete under uniaxial compression was 0.3. This might be because the water–cement content of concrete in their study was relatively low. For example, in Hong's mix proportion, the maximum water-to-binder ratio was 0.42, whereas the water-to-binder ratio in this study was 0.5. The smaller the water-to-binder ratio, the lower is the initial porosity. This results in a less compressible space for concrete and lowers the stress levels for achieving the best resistance to chloride ions.

Compared with old mortar, natural aggregates are more difficult to compress. Hence, the chloride diffusion coefficient of natural aggregate concrete is less sensitive than that of recycled concrete.

### 3.4 Predictive model of chloride diffusion coefficient

Based on the distribution of the measured test data points, a prediction model for the chloride ion diffusion coefficient of recycled concrete was established, as shown in Eq. (1). The model can predict the effects of aggregate water absorption and biaxial stress levels on the chloride ion diffusion coefficient of recycled concrete ($D_{D_{cl}}$).

$$D_{D_{cl}} = (4.93 \cdot a^{1.1} + 2.34) \cdot [2.71 \cdot \cosh(x^{1.56} - 0.29) \cdot \cosh(y^{1.56} - 0.29) - 1.69], \quad (1)$$

where $a$ is the water absorption of the aggregate; $x$ and $y$ are the stress levels in the $X$ and $Y$ axial force directions, respectively. The relationship between the measured and predicted values of the chloride diffusion coefficient under pressure is shown in Fig. 13.

Based on Fig. 13, the predicted values were generally exactly or similar to the measured data, which demonstrates the rationality of the model used in this study. Hence, this theoretical model can be used to predict the chloride diffusion coefficients of different recycled concretes under different stress levels.

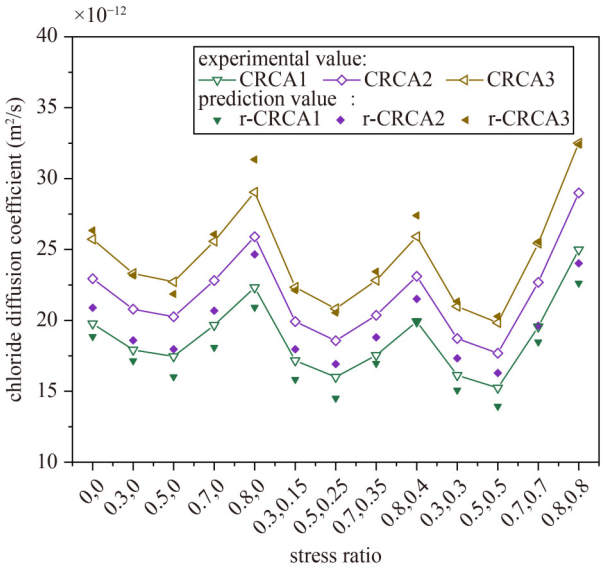


**Fig. 13** Measured and predicted values of chloride diffusion coefficient.

## 4 Conclusions

In this study, $CO_2$ was used to strengthen three types of RCAs with different water–cement ratios and cast them into recycled concrete. Subsequently, the chloride ion diffusion coefficient of the recycled concrete under a biaxial compressive load was tested. The effect of carbonization on chloride diffusion in recycled concrete under biaxial compression was explained based on a DIC strain distribution diagram and mercury pore structure distribution curve. The results indicated the following.

1) For different types of recycled concrete, whether under uniaxial compression or biaxial compression, the diffusion coefficient of chloride ions in concrete first decreased and then increased as the stress level increased. Compared with the chloride diffusion coefficient of the no-load concrete, the chloride diffusion coefficients of concrete under uniaxial and biaxial compression were 17% and 26% lower, respectively. For the same concrete mix proportion with a stress level of 0.5, the chloride diffusion coefficient in concrete under biaxial compression is 11% lower than that under uniaxial compression.

2) The chloride ion diffusion coefficient of concrete was affected by the load type and recycled aggregate quality. Carbonation improved the pore structure of the recycled aggregates, and the chloride diffusion coefficient of the recycled concrete reduced due to carbonization. For the concrete under biaxial compression with a stress ratio of 1:1, when the stress levels were 0, 0.3, 0.5, and 0.7, the chloride diffusion coefficients of recycled concrete CRCA1 were 25%, 27%, 27%, and 21% lower than those before carbonization, respectively. After carbonizing the recycled aggregates with water-to-cement ratios of 0.4, 0.5, and 0.6, the chloride diffusion coefficients of the recycled concrete under the two-axis compression above at a load level of 0.5 were 13.9, 16.3, and 20.3 ($\times 10^{-12}$ m$^2$/s), respectively.

3) When the stress level exceeded 0.5, the microcracks on the surface of concrete increased with the stress level, which is consistent with the increasing trend of the chloride ion diffusion coefficient. In this study, a

prediction model for the chloride diffusion coefficient of recycled concrete was developed. The effects of the water absorption of the aggregates and bidirectional stress level on the chloride diffusion coefficient of recycled concrete were considered in the model. The value predicted by the model was similar to the experimental value. Hence, the predictive effect of this model is favorable and can provide a reference for the durability of recycled concrete in practical engineering.

**Acknowledgements** This study was sponsored by the National Natural Science Foundation of China (Grant Nos. 52168015 and 51768005), the Natural Science Foundation of Guangxi (No. 2018GXNSFAA281333), and the Interdisciplinary Scientific Research Foundation of Guangxi University (No. 202200227).

## References

1. Zhang D. Report of the Law Enforcement Inspection Team of the Standing Committee of the National People's Congress on Inspecting the Implementation of the Law of the People's Republic of China on the Prevention and Control of Environmental Pollution by Solid Waste. Beijing: Bulletin of the Standing Committee of the National People's Congress of the People's Republic of China. 2017 (in Chinese)
2. Nassar R, Soroushian P. Use of recycled aggregate concrete in pavement construction. Journal of Solid Waste Technology Management, 2016, 42(2): 137−144
3. Watanabe T, Nishibata S, Hashimoto C, Ohtsu M. Compressive failure in concrete of recycled aggregate by acoustic emission. Construction & Building Materials, 2007, 21(3): 470−476
4. Peng G, Huang Y, Zhang J. Influence of defects in recycled aggregate on mechanical properties of recycled aggregate concrete. Journal of Building Materials, 2012, 15(1): 80−84 (in Chinese)
5. Katz A. Properties of concrete made with recycled aggregate from partially hydrated old concrete. Cement and Concrete Research, 2003, 33(5): 703−711
6. Xiao J, Li W, Sun Z, Shah S P. Crack propagation in recycled aggregate concrete under uniaxial compressive loading. ACI Materials Journal, 2012, 109(4): 451−461
7. Poon C S, Shui Z H, Lam L. Effect of microstructure of ITZ on compressive strength of concrete prepared with recycled aggregates. Construction & Building Materials, 2004, 18(6): 461−468
8. Tam V W Y, Gao X F, Tam C M. Microstructural analysis of recycled aggregate concrete produced from two-stage mixing approach. Cement and Concrete Research, 2005, 35(6): 1195−1203
9. Lee G C, Choi H B. Study on interfacial transition zone properties of recycled aggregate by micro-hardness test. Construction & Building Materials, 2013, 40: 455−460
10. Ying J W, Huang Y J, Gao X, Qi X B, Sun Y D. Effects of coarse and fine aggregates on long-term mechanical properties of sea sand recycled aggregate concrete. Frontiers of Structural and Civil Engineering, 2021, 15(3): 754−772
11. Evangelista L, de Brito J. Durability performance of concrete made with fine recycled concrete aggregates. Cement and Concrete Composites, 2010, 32(1): 9−14
12. Srubar W V III. Stochastic service-life modeling of chloride-induced corrosion in recycled-aggregate concrete. Cement and Concrete Composites, 2015, 55: 103−111
13. Ben Nakhi A, Alhumoud J M. Effects of recycled aggregate on concrete mix and exposure to chloride. Advances in Materials Science and Engineering, 2019, 2019: 1−7
14. Thomas J, Thaickavil N N, Wilson P M. Strength and durability of concrete containing recycled concrete aggregates. Journal of Building Engineering, 2018, 19: 349−365
15. Ma Z, Liu M, Tang Q, Liang C, Duan Z. Chloride permeability of recycled aggregate concrete under the coupling effect of freezing−thawing, elevated temperature or mechanical damage. Construction & Building Materials, 2020, 237: 117648
16. Ma Z, Li W, Wu H, Cao C. Chloride permeability of concrete mixed with activity recycled powder obtained from C&D waste. Construction & Building Materials, 2019, 199: 652−663
17. Zhang H, Zhao Y, Meng T, Shah S P. Surface treatment on recycled coarse aggregates with nanomaterials. Journal of Materials in Civil Engineering, 2016, 28(2): 04015094
18. Güneyisi E, Gesoglu M, Algin Z, Yazici H. Effect of surface treatment methods on the properties of self-compacting concrete with recycled aggregates. Construction & Building Materials, 2014, 64: 172−183
19. Zhang H R, Liu W S, Lin X J, Su S L, Zhao B J. To ameliorate the performance of recycled aggregate concrete (RAC) by pre-treating aggregate in sulfoaluminate cement slurry and water glass solution. Journal of Building Engineering, 2021, 44: 103364
20. Zhang J, Shi C, Li Y, Pan X, Poon C S, Xie Z. Performance enhancement of recycled concrete aggregates through carbonation. Journal of Materials in Civil Engineering, 2015, 27(11): 04015029
21. Kou S C, Poon C S. Enhancing the durability properties of concrete prepared with coarse recycled aggregate. Construction & Building Materials, 2012, 35: 69−76
22. Prasad D, Pandey A, Kumar B. Sustainable production of recycled concrete aggregates by lime treatment and mechanical abrasion for M40 grade concrete. Construction & Building Materials, 2021, 268: 121119
23. Singh R, Nayak D, Pandey A, Kumar R, Kumar V. Effects of recycled fine aggregates on properties of concrete containing natural or recycled coarse aggregates: A comparative study. Journal of Building Engineering, 2022, 45: 103442
24. Zhang J, Shi C, Li Y, Pan X, Poon C S, Xie Z. Influence of carbonated recycled concrete aggregate on properties of cement mortar. Construction & Building Materials, 2015, 98: 1−7
25. Wu H X, Liang C F, Xiao J Z, Ma Z M. Properties and $CO_2$-curing enhancement of cement-based materials containing various sources of waste hardened cement paste powder. Journal of Building Engineering, 2021, 44: 102677
26. Gonen T, Yazicioglu S. The influence of compaction pores on sorptivity and carbonation of concrete. Construction & Building Materials, 2007, 21(5): 1040−1045
27. Zhan B, Poon C S, Liu Q, Kou S, Shi C. Experimental study on $CO_2$ curing for enhancement of recycled aggregate properties. Construction & Building Materials, 2014, 67: 3−7

28. Kou S C, Zhan B, Poon C S. Use of a $CO_2$ curing step to improve the properties of concrete prepared with recycled aggregates. Cement and Concrete Composites, 2014, 45: 22−28
29. Shi C, Wu Z, Cao Z, Ling T C, Zheng J. Performance of mortar prepared with recycled concrete aggregate enhanced by $CO_2$ and pozzolan slurry. Cement and Concrete Composites, 2018, 86: 130−138
30. Liang C, Ma H, Pan Y, Ma Z, Duan Z, He Z. Chloride permeability and the caused steel corrosion in the concrete with carbonated recycled aggregate. Construction & Building Materials, 2019, 218: 506−518
31. Wang J, Zhang J, Cao D, Dang H, Ding B. Comparison of recycled aggregate treatment methods on the performance for recycled concrete. Construction & Building Materials, 2020, 234: 117366
32. Mu S, De Schutter G, Ma B. Non-steady state chloride diffusion in concrete with different crack densities. Materials and Structures, 2013, 46(1−2): 123−133
33. Zhang J, Liu Y, Shi Z. Diffusion property of chloride in cracked concrete. Journal of Building Materials, 2018, 21(2): 299−303 (in Chinese)
34. Xu F, Yang Z, Liu W, Wang S, Zhang H. Experimental investigation on the effect of sulfate attack on chloride diffusivity of cracked concrete subjected to composite solution. Construction & Building Materials, 2020, 237: 107366
35. Ismail M, Toumi A, Francois R, Gagne R. Effect of crack opening on the local diffusion of chloride in cracked mortar samples. Cement and Concrete Research, 2008, 38(8−9): 1106−1111
36. Wang Q, Zhang G, Tong Y, Gu C. A numerical study on chloride diffusion in cracked concrete. Crystals, 2021, 11(7): 742
37. Lim C C, Gowripalan N, Sirivivatnanon V. Microcracking and chloride permeability of concrete under uniaxial compression. Cement and Concrete Composites, 2000, 22(5): 353−360
38. Wang H L, Dai J G, Sun X Y, Zhang X L. Time-dependent and stress-dependent chloride diffusivity of concrete subjected to sustained compressive loading. Journal of Materials in Civil Engineering, 2016, 28(8): 04016059
39. Tang J, Wu J, Wang W, Wang Z, Wu G. Effect of curing age on chloride diffusion coefficient of recycled aggregate concrete subjected to compressive stresses. Transactions of Nanjing University of Aeronautics & Astronautics, 2018, 35(2): 326−333
40. Zhou Q, Lu C, Wang W, Wei S, Lu C, Hao M. Effect of fly ash and sustained uniaxial compressive loading on chloride diffusion in concrete. Journal of Building Engineering, 2020, 31: 101394
41. Wang W, Wu J, Wang Z, Wu G, Yue A. Chloride diffusion coefficient of recycled aggregate concrete under compressive loading. Materials and Structures, 2016, 49(11): 4729−4736
42. Hong L, Cheng W, Wang S. Influence of two-way load on chloride permeability of high performance concrete. Journal of Building Materials, 2012, 15(6): 852−856 (in Chinese)
43. Cheng X, Peng J, Cai C S, Zhang J. Experimental study on chloride ion diffusion in concrete under uniaxial and biaxial sustained stress. Materials (Basel), 2020, 13(24): 5717
44. JGJ 52-2006. Standard for Technical Requirements and Test Method of Sand and Crushed Stone (or Gravel) for Ordinary Concrete. Beijing: China Architecture & Building Press, 2006 (in Chinese)
45. Ying J, Qian S, Qing S. Chloride diffusion law in recycled concrete under biaxial compression. Journal of Architecture and Civil Engineering, 2021, 38(2): 90−98 (in Chinese)
46. GB/T 50082-2009. Standard for Test Methods of Long-Term Performance and Durability of Ordinary Concrete. Beijing: China Architecture & Building Press, 2009 (in Chinese)
47. Mehta P K, Monteiro P. Concrete: Microstructure, Properties, and Materials. New York: McGraw-Hill, 2006
48. Yang C C. On the relationship between pore structure and chloride diffusivity from accelerated chloride migration test in cement-based materials. Cement and Concrete Research, 2006, 36(7): 1304−1311
49. Zhang M, Li H. Pore structure and chloride permeability of concrete containing nano-particles for pavement. Construction & Building Materials, 2011, 25(2): 608−616
50. Chen T F, Gao X J. Effect of carbonation curing regime on strength and microstructure of Portland cement paste. Journal of $CO_2$ Utilization, 2019, 34: 74−86
51. Li W, Xiao J, Sun Z, Shah S P. Failure processes of modeled recycled aggregate concrete under uniaxial compression. Cement and Concrete Composites, 2012, 34(10): 1149−1158
52. Xiao J, Li W, Corr D J, Shah S P. Effects of interfacial transition zones on the stress−strain behavior of modeled recycled aggregate concrete. Cement and Concrete Research, 2013, 52: 82−99
53. Li W, Long C, Tam V W Y, Poon C S, Duan W H. Effects of nano-particles on failure process and microstructural properties of recycled aggregate concrete. Construction & Building Materials, 2017, 142: 42−50
54. Ying J, Zhou B, Xiao J. Pore structure and chloride diffusivity of recycled aggregate concrete with nano-$SiO_2$ and nano-$TiO_2$. Construction & Building Materials, 2017, 150: 49−55
55. Zhan B J, Xuan D X, Zeng W L, Poon C S. Carbonation treatment of recycled concrete aggregate: Effect on transport properties and steel corrosion of recycled aggregate concrete. Cement and Concrete Composites, 2019, 104: 103360
56. Chang H L. Chloride binding capacity of pastes influenced by carbonation under three conditions. Cement and Concrete Composites, 2017, 84: 1−9